Subnanosecond Thomson scattering on a vacuum arc discharge in tin vapor

E. R. Kieft and J. J. A. M. van der Mullen*
Department of Applied Physics, Eindhoven University of Technology, P.O. Box 513, 5600 MB Eindhoven, The Netherlands

V. Banine
ASML Netherlands B.V., De Run 6501, 5504 DR Veldhoven, The Netherlands

(Received 23 May 2005; published 31 August 2005)

In a previous series of Thomson scattering (TS) experiments on an extreme ultraviolet producing vacuum arc discharge in tin vapor, background radiation emitted by the plasma was found to make measurements impossible for all parts of the discharge except the prepinch phase. To reduce the level of recorded background radiation, we have built a setup for time and space resolved subnanosecond TS. Results obtained with this new setup are presented for experiments on previously inaccessible parts of the discharge—the ignition phase, pinch phase, and decay phase. For the first two, measurements have been performed at different heights in the plasma. Electron densities for the pinch phase have been derived. For the decay phase, the electron densities confirm previous Stark broadening data. From the overall results, a more complete picture of the plasma evolution can be formed.

DOI: 10.1103/PhysRevE.72.026415 PACS number(s): 52.25.Os, 42.62.Fi, 52.70.Kz, 52.80.−s

I. INTRODUCTION

Several types of pulsed discharge plasmas have in recent years attracted attention due to their capability of emitting extreme ultraviolet (EUV) radiation relatively efficiently; see, e.g., Refs. [1–6]. This capability makes them potential candidate light sources for the next generation of semiconductor lithography, in which high-power sources of radiation in a 2% band around 13.5 nm are required. Certain types are being developed further to improve their characteristics in, among others, the fields of output power, lifetime, and cleanliness (see, e.g., Refs. [7,8] and several contributions in Ref. [9]).

In further development and optimization of EUV producing discharges, a better understanding of the discharge evolution can be of great help. Such understanding could come from direct observation, or from the results of computer modeling. However, computer models in general need measurements of plasma parameters—such as electron temperatures and densities—to test their validity.

One specific type of discharge plasma is a laser-triggered vacuum arc discharge in tin vapor. In our EUV Laboratory at ASML, an experimental version of such a type of source, originally from the Institute of Spectroscopy of the Russian Academy of Sciences (ISAN) in Troitsk, Russia, has been in operation since early 2003. Results from time-resolved imaging and spectrometry in the EUV range on the plasma have been presented in Ref. [10]. The setup consists of two electrodes, of which the cathode (the bottom electrode), is covered with a layer of liquid tin. Both electrodes are electrically connected to a ring of capacitors and separated by a vacuum, or a background gas at very low pressure. See Fig. 1 for a schematic picture. Before the start of the discharge, the capacitors are charged to a potential of 4 kV. Figure 2 shows a typical plot of the electric current during the discharge pulse. The pulse evolution can be described by splitting it up into four main phases, which will be briefly described here.

In the *ignition* phase (1), caused by the firing of a laser pulse onto the surface of the cathode, a plume of vaporized and partly ionized tin expands into the vacuum until it reaches the edge of the anode. As soon as a sufficiently conducting path has been created, a discharge starts, and an electric current heats and ionizes the tin plasma further—the *prepinch* phase (2). Under influence of the azimuthal magnetic field, associated with the strong electric current, the plasma starts to compress in the radial direction, until it finally reaches a narrow, elongated shape: the *pinch* phase (3). Due to the increase in density that is caused by the compression, the emission of EUV radiation is strongest in this phase. Because of the lack of confinement of the plasma in the axial direction (as the magnetic field confines the plasma only in the radial direction), and the finite amount of energy stored in the capacitors connected to the electrodes, the plasma quickly starts to expand and decay—the *decay* phase (4)—until finally vacuum between the electrodes is restored for the next discharge pulse.

Apart from the measurements mentioned above, two types of plasma diagnostics have been applied to characterize the

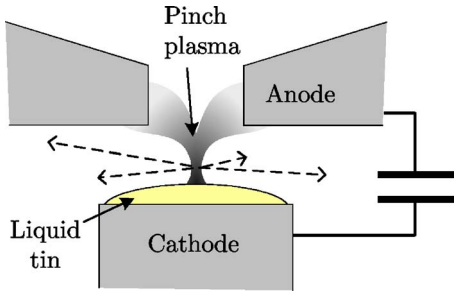

FIG. 1. A schematic cross section of the discharge electrodes. The curved shape in the center represents the pinch plasma.

*Electronic address: j.j.a.m.v.d.mullen@tue.nl

evolution of the plasma of this source; these are Stark broadening [11] and Thomson scattering (TS) [12].

Stark broadening of spectral lines of tin ions was used to measure electron densities. Spatially resolved measurements were difficult to perform since, as it is a passive spectroscopic technique, measurements are always over a line of sight. Fortunately, the intensity of the line radiation is strongly dependent on the local density, so that the spectrum measured along a line through the center of the plasma quite closely represents the peak electron density in a cross section of the plasma.

Spatially resolved measurements are more straightforward with TS, an active spectroscopic technique. A laser pulse is fired into the plasma, and the spectrum of light that is scattered by free electrons is recorded, and, after processing, compared to a theoretical spectrum. With this technique, not only electron densities, but also temperatures can be measured. Results for the prepinch phase of the tin vapor discharge have been presented in Ref. [12]. The applicability of this technique was limited to the prepinch phase, since in the other parts the accurate determination of the TS spectrum was impossible. The cause was random fluctuations in the level of background radiation, emitted by the plasma itself. Yet, measurements for these other phases were desired to obtain a more complete picture of the plasma evolution. The ratio of the TS signal to the background level would have to be improved to make reliable measurements for the other phases possible.

Given the possibility of plasma disturbance by the laser, a simple further increase of the laser pulse energy (which is, in principle, proportional to the detected TS signal intensity) was undesirable. If the TS signal intensity could not be increased, the level of background radiation would have to be lowered. Our main approach to achieve this was to reduce the time that is needed to record a single measurement. For this, we have designed and built a new setup for subnanosecond Thomson scattering. Details on this design and characterization of the final setup will be given elsewhere [13].

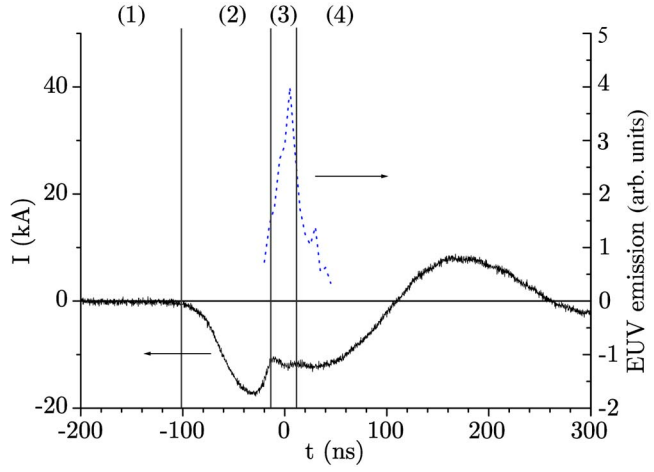

FIG. 2. Typical electrical current (solid curve) and relative EUV emission as derived from plasma imaging [10] (dotted curve), as a function of time during the discharge pulse. The numbers at the top correspond to the discharge phases as listed in the text.

In this paper, we present the results of subnanosecond Thomson scattering on the tin vapor discharge. First, in Sec. II, properties of the new setup are summarized, and the experimental procedure is explained. In Sec. III, the experimental results are presented and discussed separately for the decay phase, the ignition and prepinch phases, and the pinch phase of the discharge, respectively. Finally, our main conclusions are summarized.

II. EXPERIMENT

Thomson scattering experiments can give information about electron densities and temperatures in a plasma simultaneously. In this technique, a laser pulse is focused into a plasma, and the light scattered by free electrons is recorded. A double Doppler shift due to the velocities of the electrons causes a broadening of the spectrum of the scattered light. In the case of a Maxwellian electron energy distribution and noncollective scattering, the resulting spectrum has a Gaussian shape, the width of which is directly related to the electron temperature. The intensity of the scattered light is a measure of the electron density. On the other hand, at sufficiently high ratios of electron density over electron temperature, n_e/T_e, the scattering process is *collective*. In the collective scattering limit, the laser light is scattered off plasma waves rather than individual electrons, and sharp peaks are found in the scattered spectrum that are separated from the central laser frequency by the plasma frequency. For the intermediate case of *partially* collective scattering, the shape of the spectrum is given by the Salpeter approximation [14]. In this case, compared to noncollective scattering, not only the total scattered intensity but also the shape of the spectrum provides information on the electron density. The degree of collectivity is determined by the so-called *scattering parameter* α, which depends on the ratio n_e/T_e as indicated above.

In our setup, we combine a laser with 150 ps pulse duration, the SL 312 from Ekspla, with the 4Picos camera from Stanford Computer Optics, which has a minimum gate width of 200 ps. The laser is a frequency-doubled neodymium-doped yttrium aluminum garnet (Nd:YAG) laser at 532 nm. A photodiode signal is used to synchronize the camera to the laser pulse; an optical delay line on the laser table provides enough time for the operation of the triggering electronics of the camera. In our experiments, the laser pulse energy in the plasma was limited to 50 mJ; the pulse energy directly from the laser had to be somewhat higher due to losses in the optical path of the laser beam. The waist diameter of the laser focus was measured to be about 150 μm.

We used a triple grating spectrograph (the TGS-II) to record the Thomson scattered light. The design of this spectrograph was based on the original design of the setup built by Van de Sande [15]. In this design, three separate spectrographs are placed in series. The first two are arranged in a subtractive configuration. A notch or edge mask is located behind the first spectrograph, and an intermediate slit behind the second. In this arrangement, the first two spectrographs serve as a powerful stray light filter. In our case, the maximum achievable spatial and spectral resolution of the spectrograph are about 70 μm and 0.4 nm, respectively. The low-

est electron temperature that can be measured reliably with this setup is about 1 eV.

The TGS-II covers a wavelength range of about 50 nm width in total. The actual range can be changed by an appropriate rotation of the three gratings; either the entire TS spectrum can be recorded symmetrically up to 25 nm from the central wavelength on both sides, or only one side of the spectrum can be covered up to 50 nm from the central wavelength. This is done when particularly broad spectra are expected.

The procedure for recording of the TS spectra and their subsequent processing was largely similar to the procedure followed for our previous experiments [12]. First of all, before each series of experiments, we recorded a spectrum of rotational Raman scattering in nitrogen gas, in order to obtain an absolute intensity calibration of the system.

Further, during TS experiments, a rotatable polarization filter in front of the camera was used to separate the plasma background from the TS signal. Here, we made use of the fact that the Thomson scattered light has only one polarization direction, while in principle, the background is unpolarized. We measured a signal for two orthogonal polarizations both with the laser pulse present, and subtracted one signal from the other to obtain just the Thomson spectrum. This way, we could eliminate any systematic effect that the presence of the laser pulse may have on the emitted plasma spectrum. Before subtraction, both signals were corrected for the polarization and wavelength dependent sensitivity of the TGS-II.

In our experiments, recorded signals from typically 100 laser shots were integrated to form one camera image, to partially average out the background fluctuations. Pixels in the camera images were grouped in both spatial and spectral directions, to form new "superpixels" which have a size that roughly matches the resolution of the system, namely 181 μm (spatially) $\times 0.34$ nm (spectrally). This procedure, called binning, reduces the noise in the signal and the amount of data to be processed. After binning, each image was corrected for the corresponding polarization-dependent sensitivity, and the background subtraction was performed.

Next, for each horizontal position along the laser beam, the obtained TS spectrum was fitted to the theoretical curve, giving the local electron temperature T_e and density n_e. For the theoretical shape of the curve we used the Salpeter approximation [14], with a numerical approximation for the plasma dispersion function. More details on the fit function are given in Ref. [12].

Even though an absolute intensity calibration from rotational Raman scattering was available, the total scattered intensity was typically left as an additional free parameter, the *intensity factor* ξ. In other words, n_e and T_e were derived from just the *shape* and *width* of the spectrum, without actually using the integrated intensity. Thus errors that may be present in the calibration experiment and those that are caused by alignment drifts during TS experiments, could be avoided. This was possible because of the relatively large values of the scattering parameter, $0.6 < \alpha < 2.3$, in nearly all cases.

The intensity factor is further influenced by the spatial and temporal gradients and jitter of the plasma. In the ideal case, ξ would always be unity—that is, the measured intensities would be exactly equal to the theoretical ones. However, if, for example, a plasma of certain density is hit by the laser pulse in only 50% of all shots, an intensity factor $\xi = 0.5$ results. Now, the directly fitted electron density $n_{e,fit}$ represents the actual density in the plasma. On the other hand, the *effective* density $n_{e,eff} = \xi n_{e,fit}$ represents the density averaged over all shots, including the ones in which the plasma was "missed."

In the limit of noncollective scattering, the effects of ξ and $n_{e,fit}$ on the spectrum cannot be separated, and only their product $n_{e,eff}$ provides a meaningful number. In such cases (typically when α was smaller than about 0.6), ξ was kept fixed during the fitting procedure. The same thing was done in a very limited number of cases in which the shape of the spectrum was particularly disturbed by background radiation. Good estimates for ξ could be derived from the values in neighboring data points.

Finally, for each time step, the maximum fitted electron density $n_{e,max}$ and a weighted average $T_{e,av}$ were determined over the entire horizontal spatial profile. For the relative weight of each T_e value, needed to calculate $T_{e,av}$, the effective density $n_{e,eff}$ at the same spatial position was used. $n_{e,max}$ and $T_{e,av}$ could be used to characterize the plasma as a function of time during the discharge pulse.

In this procedure, only the relative values of ξ within each spatial profile are relevant, and the absolute values are not important. However, it is worth mentioning that within each profile, the maximum value of ξ was typically between 0.4 and 0.8. The difference from unity can be ascribed partly to some instability of the discharge, but mainly to a certain drift of the alignment of the setup during each experiment. In most cases, the value of ξ was lower at the sides of the profile than in the center, which could be the result of some positional instability of the plasma, or of the dynamical processes of expansion and compression that take place in the plasma evolution.

III. RESULTS

In the following three sections, the experimental results will be discussed for the decay phase, the ignition and prepinch phases, and the pinch phase, respectively.

A. Decay phase

The results of a scan through the decay phase of the discharge have been plotted in Fig. 3. For this scan, the wavelength range of 507–557 nm was used. In the same plot, results from previous Stark broadening measurements, as presented in Ref. [11], are shown.

It is interesting to see that the TS measurements closely reproduce the Stark densities in the decay phase; even some detailed features in the shape of the curve between $t=1$ and 2 μs can be recognized. It is worth mentioning that the decay of the electron density is much slower than would be expected from a simple expansion of the pinch plasma; the main cause is additional evaporation of tin from the cathode surface due to the energy absorbed during the discharge—as

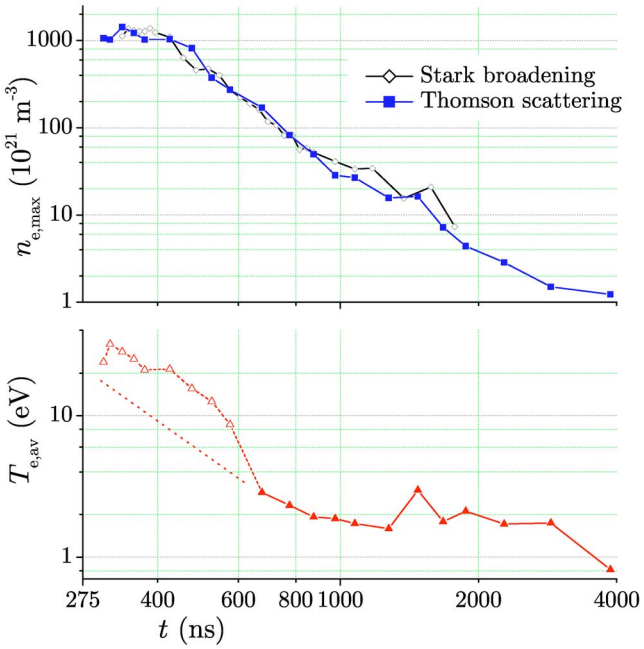

FIG. 3. Electron densities and temperatures in the decay phase, as measured using Thomson scattering, and electron densities from Stark broadening. The time is relative to the ignition laser pulse; pinching occurs around $t=250$ ns, or just before the start of the axis. The first part of the T_e data is represented by a dashed line to indicate that in these measurements the results may be influenced by absorption of laser light.

observed in Ref. [10]. Further, an oscillating electric current between both electrodes is still present and still delivers energy to the plasma in this phase.

In our previous paper on Thomson scattering [12] the possible influence of laser absorption on the plasma has already been mentioned. The possible effect of laser energy absorption in line transitions (as discussed there for the early prepinch phase) of Sn ions is also present here, and could lead to a detectable increase of n_e of about 30% in the most extreme case. However, given the good match with the Stark broadening results (for which no laser pulse was present), the effect seems to be very limited here.

On the other hand, it is likely that laser absorption has significantly influenced the electron temperature in the early decay phase (about 0.3–0.6 μs on the time scale). For this part, one would expect a lower temperature, such as suggested by the dotted line in Fig. 3. The main reasons to expect a lower temperature are the additional evaporation of tin, as mentioned above, which would lead to a relatively cool plasma; the presence of strong line radiation of relatively low ionization stages of tin—which can only exist if the temperature is not too high; and the absence of strong EUV emission in other experiments at this time in the evolution of the discharge [10].

In order to verify the laser-induced increase of T_e, we have performed separate laser absorption measurements. These revealed absorption of up to 4% of the laser pulse energy in the early decay phase. This number corresponds to an energy addition of 2 mJ to the plasma. If we assume an electron density of 1.5×10^{24} m^{-3}, a total length for absorption of about $l=5$ mm, an average beam diameter of $r=100$ μm, and an increase of the electron temperature by 15 eV, the energy needed for electron heating amounts to

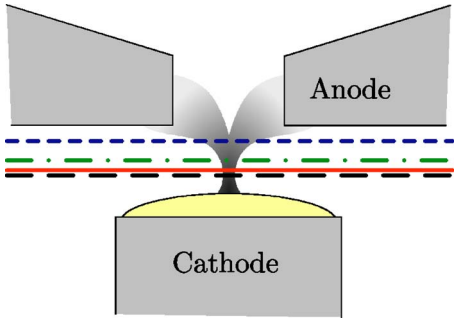

FIG. 4. Cross section of the discharge electrodes, with horizontal lines corresponding to the laser beam positions for different TS experiments. The different line patterns match those of the plots in Fig. 5. Distances from the cathode are, from bottom to top, 0.65, 0.85, 1.2, and 1.9 mm.

$$E = n_e l \pi r^2 \frac{3}{2} k_B \Delta T_e = 0.85 \text{ mJ}, \quad (1)$$

a number that is somewhat smaller than the 2 mJ reported above. However, the electron temperature increase as derived from Fig. 3 is an effective number integrated over the laser pulse. The accumulated temperature increase at the end of the pulse could be larger than this value. Further, the increase in excitation and ionization of Sn atoms and ions, as mentioned above, could form another, although probably smaller, destination for the absorbed laser energy. In other words, the actual heat capacity of the plasma is larger than the value used in Eq. (1) above.

B. Ignition and prepinch phases

To study the ignition and prepinch phases in more detail, measurements have been done for different vertical positions in the plasma (or, equivalently, different distances to the cathode). The cross sections of the plasma for the different experimental series are depicted schematically in Fig. 4. For these measurements and those presented in the following section, the spectrograph alignment was shifted to the wavelength range of 482–532 nm. This is because of the high electron densities that were expected for the pinch phase, which, in the case of collective TS, lead to spectra that extend far away from the laser wavelength (see the next section). The lower half of the spectrum (in the wavelength domain) was chosen rather than the higher one, since it appeared to have a more "clean" background spectrum.

In Fig. 5, the results from these experiments are represented by the various patterned lines. From these plots, it can be clearly observed that a plasma appears first near the cathode, a relatively short time after the ignition laser pulse was fired. Later, while at the lowest positions the electron density and temperature are decreasing somewhat, a less dense and colder part of the plasma appears further away from the cathode. From the density plots, a velocity of the plasma front of about 2×10^4 m s^{-1} can be derived.

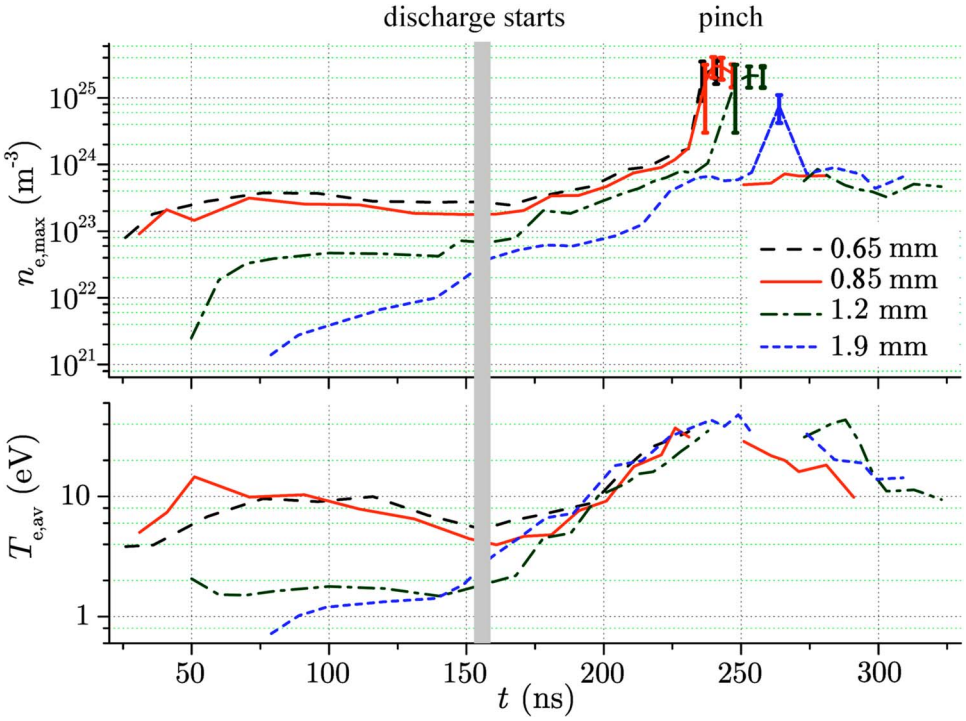

FIG. 5. Electron densities and temperatures derived from Thomson scattering, as a function of time (relative to the ignition laser pulse) and for different heights in the plasma. The various patterned lines correspond to measurements in the ignition and prepinch phases; the vertical bars represent density measurements for the pinch phase.

Further, it can be concluded that the electron density near the anode reaches a few times 10^{22} m^{-3} before the discharge starts. The moment of the start of the discharge was detected by a current probe, but it can also be derived from the fact that at this time, the electron temperature near the cathode starts to increase again—which is most likely caused by ohmic heating due to the electric current. The electric current leads to fast ionization and heating of the plasma. In the second half of the prepinch phase, compression of the plasma starts to contribute to a further increase of electron density. To illustrate this, the plasma radius derived from background radiation for one of the experimental series has been plotted in Fig. 6.

In Ref. [12] it was mentioned that the electron temperature in the prepinch phase generally has a "hollow" shape. This phenomenon has been confirmed by our new experiments. It is more pronounced in the higher profiles, as these have lower temperatures at the start of the electric current. By contrast, the profiles of the laser-induced plasma in the ignition phase have their highest electron temperatures in the center. Examples of density and temperature profiles are shown in Fig. 7.

Like in the decay phase, illumination by the laser may cause a small relative density increase in the ignition phase and the first part of the prepinch phase. Theoretically, it is the strongest in a high density, cool (1 to 2 eV) plasma. In our results, we have either low densities or higher electron temperatures, so that the effect is probably very limited. Also, the influence on T_e is expected to be very small in this case, as on the one hand the particle densities are much lower than in the decay phase, and on the other hand, the pulse duration of the laser is much shorter than in the previous experiments, so that there is much less time available for electron heating.

C. Pinch phase

In the pinch phase, fitting of measured TS spectra to a theoretical spectrum, defined by single values for n_e and T_e, was found to be impossible. The duration of the pinch itself is only on the order of 10 ns, and the diameter is around 200 μm or less. Therefore both spatial and temporal gradients of the plasma parameters are very large. Even gradients of n_e and T_e *across* the laser beam can be significant. Also,

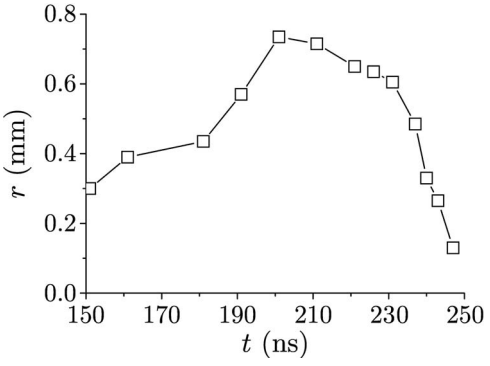

FIG. 6. Plasma radius derived from the background radiation for the experimental series recorded at 0.85 mm from the cathode. Compression already starts around $t=200$ ns, but becomes much stronger only after $t=230$ ns. Note that for the last data point, the measured radius may be limited by the resolution of the spectrometer.

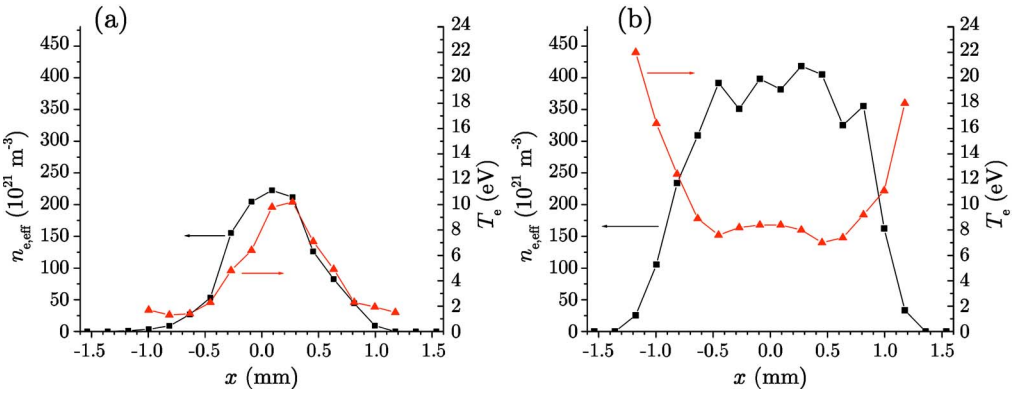

FIG. 7. Effective electron density (square) and temperature (triangle) profiles for two measurements in the ignition and prepinch phases. (a) Recorded at $t=136$ ns in the ignition phase; (b) at $t=196$ ns, in the prepinch phase. Both profile pairs were taken from the experimental series at the lowest vertical position.

jitter in the timing (~3–5 ns) and spatial position of the pinch plasma is present and plays a significant role. Hence the recorded signal is always a mixture of signals from regions or periods of time with different densities and temperatures.

Theoretically, for the plasma parameters expected for this part of the discharge, almost the complete electron contribution to the TS intensity is concentrated in sharp peaks separated from the central laser frequency by the plasma frequency, which is a function of the electron density only. Therefore the electron density could be determined just from recording the position of the peak in the spectrum.

In practice, the sharp peak at the plasma frequency is "smeared out" to a broader feature, reflecting an electron density *distribution* rather than a single value. An example of such a spectrum is shown in Fig. 8. Similar distributions have been recorded for different distances from the cathode, and they have been found for different positions on the time scale. The upper and lower limits of these distributions are indicated by the vertical bars in Fig. 5.

Two trends can be observed in the results: first, the time at which the pinch effect occurs depends on the height in the plasma; pinching is slower at higher positions. This is known as the "zippering effect," which is caused by the fact that the magnetic field in the plasma varies with height. Second, the densities in the pinch seem to decrease with distance from the cathode. The central density of the distribution varies from $n_e=3.1\times10^{25}$ m^{-3} near the cathode to 0.8×10^{25} m^{-3} close to the anode. This reflects the fact that already at the start of the discharge, the atomic density of tin is highest near the cathode, so that at this position, more material is available for the pinch plasma.

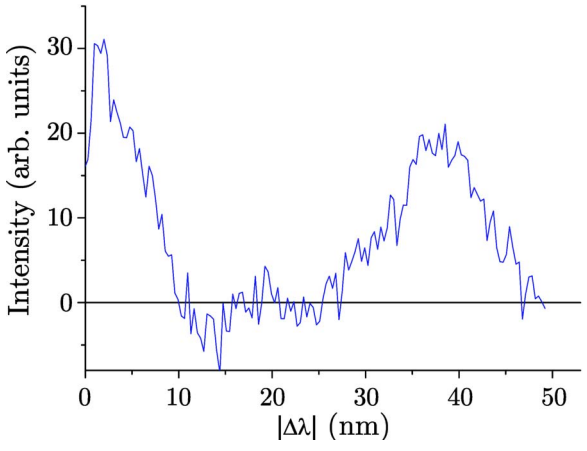

FIG. 8. Example of a recorded Thomson spectrum for the pinch phase. The feature at $|\Delta\lambda|<10$ nm can be partially ascribed to Thomson scattering from a low-density plasma around the pinch, and could also be affected by imperfect background subtraction and/or stray light blocking.

Averaged electron temperatures could in principle be determined from the integrated intensities of the spectra. This follows from the fact that, in the limit of strongly collective scattering, the TS intensity tends to a constant factor times the electron temperature. However, plasma jitter and gradients, and alignment imperfections, also affect the measured intensity. Further, the method would be highly sensitive to any signal offset that remains after background subtraction, which is a relatively difficult procedure in this phase. Finally, inverse bremsstrahlung absorption of laser radiation could become significant for the highest recorded electron densities; theoretically, it could lead to a temperature increase of up to about 10 eV. Therefore we did not attempt to perform actual electron temperature measurements. However, in general, the intensities are roughly consistent with T_e values of 25–40 eV.

IV. CONCLUSIONS

After our previous findings from Thomson scattering experiments on a tin vapor discharge in the prepinch phase, we have designed and built a new setup for subnanosecond Thomson scattering. With the new setup, we have been capable of probing parts of the discharge that were previously inaccessible to Thomson scattering experiments. The evolution of the tin vapor discharge has now been described more quantitatively and in more detail, especially for all parts of the discharge other than the prepinch phase.

Specifically, for the ignition phase we have found electron densities and temperatures near the cathode of up to 2×10^{23} m^{-3} and around 10 eV, respectively, while those further away from the cathode both were much lower, and in

fact, the discharge current did not start until the density near the anode reached about 2×10^{22} m^{-3}. Next, the plasma behavior in the prepinch phase roughly followed the results already found in our previous work. We can now confirm that the fast increase in electron density is both the result of further ionization and the onset of plasma compression. Another effect, the hollow temperature profile, has also been confirmed, and it was found that it is strongest further away from the cathode, and that a similar effect is not present in the ignition phase. We have been able to determine electron densities for the pinch phase of the discharge, and have found that these decrease with distance from the cathode. Further, the time of pinching increases with distance from the cathode. Finally, electron density measurements for the decay phase provided an independent conformation of the Stark broadening results for a regime for which they were not previously available. At the same time, the good match with Stark broadening data is an indication that additional ionization due to the presence of the laser pulse is limited.

Some limitations were found for the interpretation of the TS results, though. Care should be taken especially in those cases where strong line radiation is present. Further, although it was possible to probe both electron densities and temperatures in the compressing plasma, once the pinch plasma has reached its final, narrow radius, inherent gradients and plasma jitter were found to make independent determination of the electron temperature practically impossible.

However, in general, we have demonstrated that it is possible to measure extremely wide ranges of n_e and T_e values (over more than four, and almost two orders of magnitude, respectively) in what is basically a single experiment.

[1] M. A. Klosner and W. T. Silfvast, Opt. Lett. **23**, 1609 (1998).
[2] W. N. Partlo, I. V. Fomenkov, R. Oliver, and D. L. Birx, Proc. SPIE **3997**, 136 (2000).
[3] V. M. Borisov, I. Ahmad, S. Götze, A. S. Ivanov, O. B. Khristoforov, J. Kleinschmidt, V. Korobotchko, J. Ringling, G. Schriever, U. Stamm, and A. Y. Vinokhodov, Proc. SPIE **4688**, 627 (2002).
[4] M. McGeoch, Appl. Opt. **37**, 1651 (1998).
[5] M. McGeoch and C. Pike, in *Proceedings of the EUV Source Work-shop, International SEMATECH, Dallas, TX, 2002*, edited by V. Bakshi, http://www.sematech.org/resources/litho/meetings/euvl/20021014/10-PLEXLLC.pdf.
[6] K. Bergmann, G. Schriever, O. Rosier, M. Müller, W. Neff, and R. Lebert, Appl. Opt. **38**, 5413 (1999).
[7] M. McGeoch, J. Phys. D **37**, 3277 (2004).
[8] U. Stamm, J. Phys. D **37**, 3244 (2004).
[9] Proceedings of the 3rd International EUVL Symposium, Miyazaki, Japan, edited by V. Bakshi (Sematech, Austin,TX, 2004).
[10] E. R. Kieft, J. J. A. M. van der Mullen, G. M. W. Kroesen, V. Banine, and K. N. Koshelev, Phys. Rev. E **71**, 026409 (2005).
[11] E. R. Kieft, J. J. A. M. van der Mullen, G. M. W. Kroesen, V. Banine, and K. N. Koshelev, Phys. Rev. E **70**, 066402 (2004).
[12] E. R. Kieft, J. J. A. M. van der Mullen, G. M. W. Kroesen, V. Banine, and K. N. Koshelev, Phys. Rev. E **70**, 056413 (2004).
[13] E. R. Kieft, C. H. J. M. Groothuis, J. J. A. M. van der Mullen, and V. Banine, Rev. Sci. Instrum. (to be published).
[14] E. E. Salpeter, Phys. Rev. **120**, 1528 (1960).
[15] M. J. van de Sande, Ph.D. thesis, Eindhoven University of Technology, 2002, http://alexandria.tue.nl/extra2/200210414.pdf